Structure of void space in polymer solutions

Bong June Sung
Department of Chemistry, Sogang University, Seoul 121-742, Republic of Korea

Arun Yethiraj
Department of Chemistry and Theoretical Chemistry Institute, University of Wisconsin, Madison, Wisconsin 53706, USA

(Received 30 June 2009; revised manuscript received 21 December 2009; published 8 March 2010)

The structure of void space in two- and three-dimensional (3D) polymer solutions is studied using Voronoi tessellation and percolation theory. The polymer molecules are modeled as freely jointed chains of N tangent hard disks (two dimensions) or spheres (three dimensions). Polymer chains are equilibrated via Monte Carlo simulations and the pore space in configurations of equilibrated chains is mapped using Voronoi tessellation. In d dimensions a Voronoi vertex is the center of the sphere tangent to the $d+1$ nearest monomers. An edge of the Voronoi diagram is the shortest route between two neighboring vertices. The edge is considered connected if a monomer can pass through and disconnected otherwise. The Voronoi construction is used to calculate the percolation threshold of the void space. The most interesting result is that the polymer area fraction at the percolation threshold is a nonmonotonic function of N in two dimensions but monotonically reaches a constant value in three dimensions. The crossover behavior of the percolation threshold is also observed in pseudo-3D. The pore size distribution decreases monotonically with increasing pore size. This is markedly different from that in configurations of hard disks (monomeric fluid) where the pore size distribution is peaked at finite size.

DOI: 10.1103/PhysRevE.81.031801 PACS number(s): 61.25.H−, 68.47.Pe, 82.35.Gh

I. INTRODUCTION

The free volume (or accessible volume) is the volume in a polymer melt or solid that is accessible to penetrants. The size and connectivity of free volume determine various properties such as penetrant diffusivity, which is important in applications such as gas permeation and separation using membranes [1,2] or nanocomposites [3]. Recently, positron annihilation lifetime spectroscopy [3–6] has been used as a direct method to probe pore sizes of amorphous polymers. Computer simulations and numerical analyses [7–10] have been also conducted extensively to understand pore size distributions and pore connectivities of various polymeric materials.

In this paper we study the structure of void space in polymer solutions in two and three dimensions. While most studies of structure focus on correlations between polymer sites, little attention has been focused on the distribution and connectivity of the void space. It has been suggested, for example, that two-dimensional (2D) polymers would become disklike at a high concentration [11], although a Monte Carlo (MC) simulation study [12] suggests that 2D polymers did not become disklike at high concentrations and could even interpenetrate to some extent. Scaling exponents for chain size are relatively insensitive to the shape of the molecules in two dimensions, but the void structure or accessible area might be more sensitive to the shape.

The void space is a function of many-body structural correlations in the polymer and could be a strong function of the chain shape. For example, if polymers were disklike, the area accessible to a penetrant "inside" a polymer molecule would be isolated from the other percolating accessible area. In such a case, because longer chains should form bigger disklike molecules, both nonpercolating and percolating free areas should increase with chain length for a fixed polymer area fraction. If the polymer molecules could interpenetrate, however, the accessible area might show more complicated behavior.

In this work, we investigate polymer solutions as a model system to understand the effect of polymer structure on the pore percolation threshold and accessible area. Most of our attention is focused on 2D polymer solutions, although we present some results for three-dimensional (3D) and quasi-3D polymers for comparison. Our emphasis on 2D polymer solutions is motivated by the recent developments of 2D polymerization techniques in lipid bilayers [13,14] and liquid crystals [15]. In these studies amphiphiles or oligomers are organized into layered structures and catenated by chemical reactions to become two-dimensional polymers. In lipid bilayers the lateral diffusion coefficient of a probe molecule decreased first with an increase in the degree of polymerization, N, and did not change beyond a critical value of N [16,17]. Understanding the effect of polymer structure on accessible area would also shed light on the lateral diffusion of lipids.

There have been many computational algorithms proposed to analyze the pore structure in porous media [18–23], and the method of Voronoi tessellation [24] has been one of the popular approaches [7,8,25–36]. Voronoi tessellation divides space into nonoverlapping convex polyhedra, and differences in methods arise from the definitions of a pore and pore connectivity. Rigby and Roe [7] applied Voronoi tessellation to investigate the cavity size and shape of a polymer liquid and glass. Arizzi *et al.* [25] conducted Delaunay tessellation to polymeric glasses and investigated unoccupied volume distribution and cluster shapes. Greenfield and Theodorou [26] studied the effect of a tracer size in glass polypropylene microstructures using Voronoi tessellation. By comparing the polymer glass to a random close-packed atomic glass, they found that the average accessible volume fraction was larger in the polymer than in the atomic glass. Voronoi tessellation has also been applied to study free volume of nanoporous membranes [27,28].

In this work, we map pores in continuous space on an irregular lattice by using Voronoi tessellation and investigate

the pore percolation threshold. A Voronoi diagram is constructed for an equilibrated polymer configuration. Each convex polyhedron of the Voronoi diagram contains a monomer. In two dimensions, a pore is defined as a circle tangential to three neighbor monomers and its center is located at a Voronoi vertex. If an edge is wide enough and a monomer can move along the edge that connects two pores, the edge is determined connected. Otherwise, the edge is considered disconnected (*passage criterion*). The connected edges and vertices form a pore cluster. A percolating pore cluster is then located via a recursive algorithm that takes periodic boundary conditions into account.

Our analysis shows that in two dimensions the percolation threshold is a nonmonotonic function of N because a bigger portion of accessible area becomes nonpercolating as N is increased while the percolating accessible area is decreased significantly. This argues strongly against disklike conformations at high concentrations. In 3D solutions, however, the percolation threshold monotonically increases for short chains before reaching a constant value for $N \geq 8$. These suggest that the lipid bilayer systems [16,17] should be viewed as three dimensions rather than 2D systems.

The rest of the paper is organized as follows. The model and simulation method are described in Sec. II, results are presented and discussed in Sec. III, and conclusions are presented in Sec. IV.

II. MODEL AND SIMULATION DETAILS

Polymer solutions in two dimensions are prepared by placing chain molecules in a square of side L with periodic boundary conditions in all directions. The molecules are modeled as freely jointed tangent hard disk chains with a disk diameter $\sigma_m = \sigma$, where σ is the unit length. Each chain molecule consists of N beads ($N=1-1024$) and the number of chains (n) varies from 32 to 3072 depending on L, N, and the polymer area fraction $\phi_m \equiv Nn\pi\sigma_m^2/4L^2$. L ranges from 44.8 to 500 and ϕ_m ranges from 0.1 to 0.32. n disks of diameter, σ_m, are inserted as seeds into the simulation cell and grown into chains of a desired length, N, using a growth and equilibration algorithm [37]. In three dimensions, freely jointed tangent hard sphere chains of N beads are inserted into a cubic box of side $L \approx 17.5$. For 3D chains, N and the polymer volume fraction $\phi_m (\equiv Nn\pi\sigma_m^3/6L^3)$ range from 1 to 128 and from 0.1 to 0.31, respectively. In order to investigate the crossover behavior from two dimensions to three dimensions, we also model polymers in pseudo-3D by placing chains between two infinite smooth walls placed at $z=0$ and $z=h$. When $h=1$, the system corresponds to two dimensions. In our simulations, h changes from 1.1 to 2.

Polymer molecules are equilibrated by MC simulations. MC simulations are performed using standard Metropolis algorithm to equilibrate polymer melts. A molecule is chosen at random and random moves are attempted via translation, rotation, reptation [38], and continuum configurational bias [39] algorithms. A random move is accepted if the trial configuration does not result in an overlap with other chains and rejected otherwise. Each initial configuration is equilibrated over several runs of tens of million attempted moves. The mean-square radius of gyration $\langle R_g^2 \rangle$ is calculated from

$$\langle R_g^2 \rangle \equiv \frac{1}{Nn} \sum_i^n \sum_j^N \langle (\mathbf{r}_j^i - \mathbf{r}_{cm}^i)^2 \rangle, \tag{1}$$

where $\mathbf{r}_j^i$ is the position of bead j of a chain i, $\mathbf{r}_{cm}^i$ is the center of mass of a chain i, and $\langle \cdots \rangle$ denotes an ensemble average. The values of $\langle R_g^2 \rangle$ are found to agree well with previous simulations by Yethiraj [12]. For each set of (L, N, ϕ_m), about 100 snapshots of equilibrium configurations are collected. Voronoi tessellation is then performed for each configuration to investigate the percolation of the accessible area.

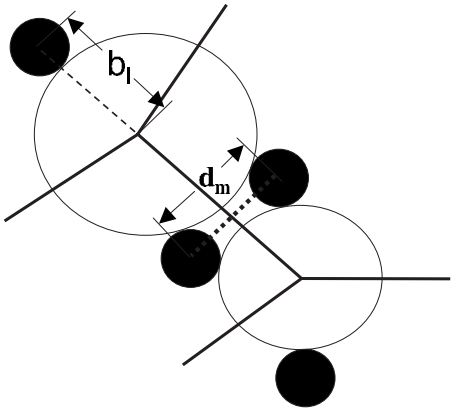

FIG. 1. A schematic figure of Voronoi tessellation of monomers (filled circles). Solid lines and empty circles represent edges of polyhedra and pores, respectively. b_l and d_m are distances between a vertex l and a monomer and between two monomers equidistant from an edge m, respectively.

In Voronoi tessellation, space is divided into many nonoverlapping convex polyhedra [24], each of which contains one monomer bead. A point in space belongs to the polyhedron of a monomer if and only if the monomer bead is the nearest one to that point. The edges and vertices of a polyhedron are equidistant from two and three monomers, respectively [34–36]. A vertex is usually an intersection of three edges and is identical to the center of a circle tangential to three monomers. The tangential circle and its diameter are defined as a pore and pore size ($\sigma_p = 2b_l - \sigma_m$), where b_l is the distance between the vertex l and the center of the nearest monomer (see Fig. 1). An edge connecting two neighbor vertices (pores) is considered as the route through which a monomer can travel between two pores. The edge width (d_m) is defined as the distance between centers of two monomers equidistant from an edge m. Once edges and vertices are determined, not only their positions but also their topological informations are stored in arrays.

After Voronoi diagram is constructed, we determine the connectivity of edges via passage criterion [34–36]. A monomer cannot move along the edge m if $d_m < \sigma_m + \sigma_f$ because the edge width is too narrow for a monomer to pass through. In this case we consider the edges disconnected. In case the width is wide enough for the monomer ($d_m \geq \sigma_m + \sigma_f$), the edge is determined a connected one. A pore cluster is defined as a set of connected edges and their vertices and is located

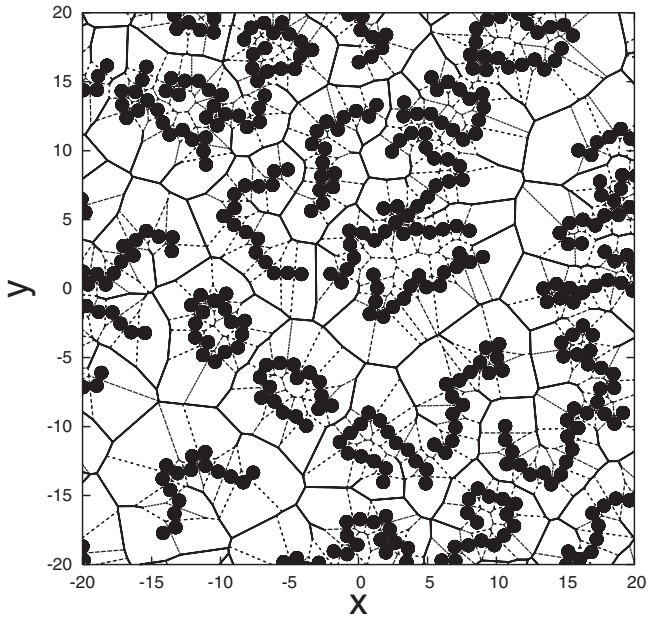

FIG. 2. A Voronoi diagram for $N=16$ and $\phi_m=0.2$. Filled circles represent monomers. Solid and dashed lines represent connected and disconnected edges of polyhedra, respectively.

via a recursive algorithm. The percolation of each pore cluster is also examined considering periodic boundary conditions. This algorithm is straightforward to apply to three-dimensional polymers [36]. In three dimensions, each pore is surrounded by a Delaunay tetrahedron with four neighbor particles at each vertex of the tetrahedron. The edge width is redefined as a diameter of a tangential circle to three particles on the face of the tetrahedron. In pseudo-3D, the smooth walls used in MC simulations are replaced by the structured walls composed of densely overlapped hard spheres. Those spheres and the configurations of polymers from MC simulations are used to construct the Voronoi diagrams in pseudo-3D. The Voronoi diagrams are tested by examining the Euler Formula, i.e., $V-E+F=2$ for every polyhedron, where V, E, and F denote the numbers of vertices, edges, and faces of each polyhedron, respectively.

A typical Voronoi diagram is depicted in Fig. 2 for $\phi_m=0.2$ and $N=16$. Solid and dashed lines represent connected and disconnected edges of polyhedra, respectively. Monomers can travel along the solid lines. Some pore clusters are isolated from a percolating pore cluster. If a monomer is placed in this isolated cluster, it would be trapped in the isolated pore cluster. When the chain length N is long enough, chains tend to form a loop inside which is isolated from a percolating cluster. Therefore, more isolated pore clusters are constructed with longer chains.

The mean cluster size $S(\phi_m,L)$ for a given system size L is defined as

$$S(\phi_m,L) \equiv \sum_{s=1}^{\infty} sP(s), \tag{2}$$

where s is the number of edges in a finite cluster and $P(s)$ is the probability that an edge belongs to a cluster containing s edges. The percolating pore cluster, if any, is excluded from this calculation. The polymer area fraction at the percolation threshold ϕ_c is identical to the peak position of $S(\phi_m,L)$ because the mean cluster size diverges at the percolation threshold when $L\to\infty$. When $\phi_m>\phi_c$, pore clusters are small. Bigger pore clusters are created and the mean cluster size is increased as ϕ_m is decreased down to ϕ_c. When $\phi_m<\phi_c$, the mean cluster size is decreased as ϕ_m is decreased because most pores belong to a percolating pore cluster and the percolating pore cluster is excluded from the calculation of the mean cluster size. Therefore, the peak position of the mean cluster size is located at the percolation threshold. As L is increased, the peak height of $S(\phi_m,L)$ increases prominently. In this work, $S(\phi_m,L)$ is averaged over about 100 polymer configurations.

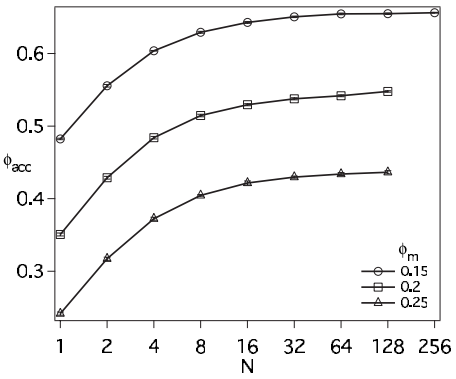

FIG. 3. Simulation results for accessible area fraction, ϕ_{acc}, as a function of N for $\phi_m=0.15$, 0.2, and 0.25.

The fraction of accessible area (ϕ_{acc}) is estimated by throwing 1×10^6 test particles with a diameter σ_f randomly in the simulation cell and calculating the fraction of nonoverlapped test particles. Similarly, the fraction ϕ_p of *percolating* accessible area for monomers is the fraction of nonoverlapped test particles whose nearest pore belongs to a percolating pore cluster. The fraction ϕ_{np} of *nonpercolating* accessible area is then defined as $\phi_{np}\equiv\phi_{acc}-\phi_p$. ϕ_{acc} and ϕ_p are averaged over ten polymer configurations.

III. RESULTS AND DISCUSSION

The majority of this section is concerned with 2D polymer solutions, where we classify space as either accessible or nonaccessible. Accessible areas are comprised of pores whose sizes are bigger than a monomer ($\sigma_p\geq\sigma_f$) so that monomers can access such areas. The accessible areas are categorized again into percolating and nonpercolating accessible areas. The percolating accessible area is the area of a percolating pore cluster. If a monomer is located in the percolating accessible area, the monomer can diffuse out through space, whereas nonpercolating accessible areas consist of isolated pore clusters; thus monomers in those are trapped.

For a given ϕ_m, the fraction of accessible area (ϕ_{acc}) increases and the nonaccessible area decreases as N is increased. This can be understood by noting that as N increases at fixed ϕ_m, the number of monomers is constant but more

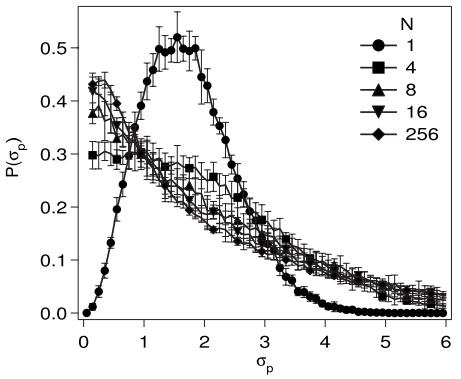

FIG. 4. Pore size distributions $[P(\sigma_p)]$ for $N=1$, 4, 8, 16, and 256 for $\phi_m=0.2$.

monomers are bonded to other monomers. When three separate monomers are located close enough to one another, it is very likely that the area surrounded by those three monomers might not be big enough for a monomer, thus becoming nonaccessible. On the other hand, if these three monomers are joined into a trimer, the probability of a large nonaccessible space is decreased. Therefore ϕ_{acc} increases with increasing N. Figure 3 depicts ϕ_{acc} as a function of N for several values of ϕ_m. For a fixed ϕ_m, ϕ_{acc} increases with N and for a fixed N, ϕ_{acc} decreases as ϕ_m is increased. This behavior was also observed in 3D polymer glasses by Greenfield and Theodorou [26]. They found that the connectivity of polymers tends to group the unoccupied volume into a few larger and many smaller clusters. This is also consistent with the fact that the pore percolation threshold of 3D polymers is different from that of monomeric media due to the larger porosity of polymers [36].

The pore size distribution $[P(\sigma_p)]$ is qualitatively different for polymeric systems when compared to systems of monomers or dimers. Figure 4 depicts $P(\sigma_p)$ for $N=1$, 4, 8, 16, and 256 and for $\phi_m=0.2$. For $N=1$ or 2, $P(\sigma_p)$ has a peak at a nonzero value of σ_p at $\sigma_p \approx 1.5\sigma$. For $N>2$, however, the peak position of $P(\sigma_p)$ shifts to $\sigma_p=0$ and the distribution narrows with increasing N. We attribute this to the fact that many small pores are constructed near a chain and the number of small pores therefore increases with N. The pore size distribution is insensitive to N for $N \geq 16$.

For small enough values of ϕ_m, the biggest pore cluster percolates throughout space. As ϕ_m increases beyond a critical value, ϕ_c, no percolating cluster exists. ϕ_c is, therefore, defined as the polymer area fraction at the pore percolation threshold and is estimated by calculating mean cluster size $S(\phi_m,L)$. At $\phi_m=\phi_c$, $S(\phi_m,L)$ diverges in the limit $L\to\infty$. In practice, we obtain $S(\phi_m,L)$ for three different values of L and obtain ϕ_c from the location of the peak.

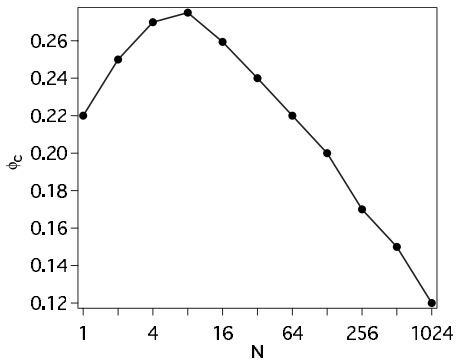

FIG. 5. Simulation results for percolation thresholds, ϕ_c, as a function of N.

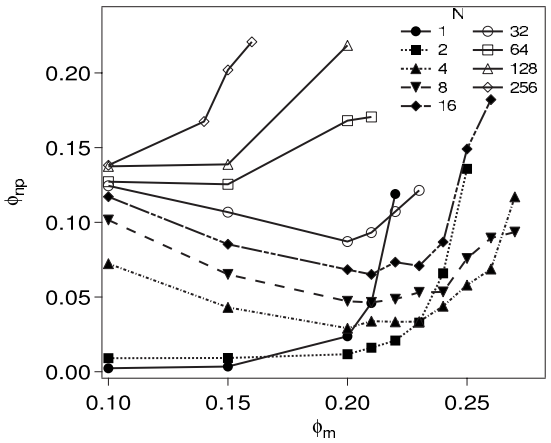

FIG. 6. Simulation results for nonpercolating accessible area fraction, ϕ_{np}, as a function of ϕ_m for $N=1-256$.

For small N, when short chains are combined to become longer chains, both the accessible area and ϕ_c increase. For infinite N, however, because the overlap area fraction (ϕ^*) goes to zero $(\phi^* \sim N/R_g^2 \sim N^{-0.5})$ and most of the accessible area is confined within the infinitely long chains, ϕ_c should decrease to zero. Therefore, the nonmonotonic behavior of ϕ_c is expected as a function of N and is observed clearly with a maximum at $N=8$ in Fig. 5. However, in our simulations ϕ_c does not appear to show the expected asymptotic behavior, which implies that the values of N studied are far from the long chain limit. From the figure, one can estimate that $\phi_c \approx 0.42N^{-0.17}$ for $N>16$. If this approximate relation holds for larger values of N, $\phi_c \approx 0.08$ only when $N \approx 10\,000$. This suggests that we would be able to observe the limiting case only for $N>10\,000$, which is well beyond our computational resources.

The nonmonotonic behavior of ϕ_c seems to conflict with the above observation that ϕ_{acc} is a monotonically increasing function of N. We plot mean cluster size as a function of ϕ_{acc}

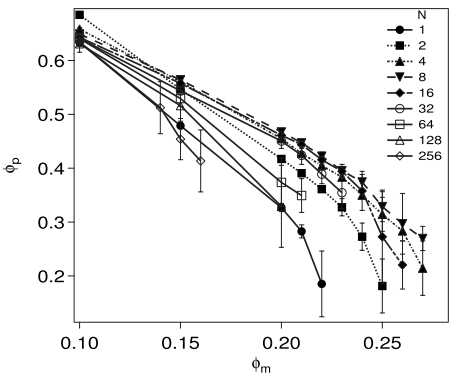

FIG. 7. Simulation results for percolating accessible area fraction, ϕ_p, as a function of ϕ_m for $N=1-256$.

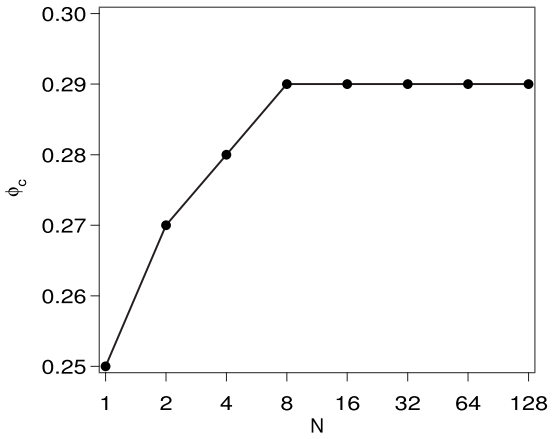

FIG. 8. Simulation results for percolation thresholds, ϕ_c, as a function of N for three-dimensional polymer solutions.

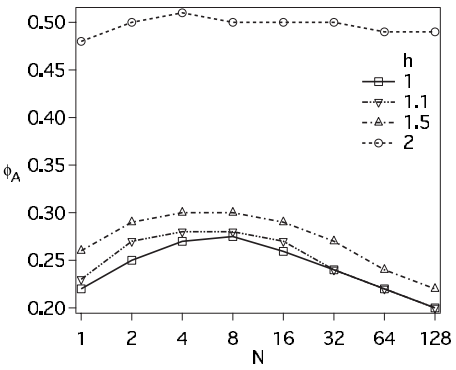

FIG. 9. Simulation results for the pseudopercolation threshold area fractions, ϕ_A, as a function of N for different values of the finite thickness (h) in pseudo-3D.

instead of ϕ_m (not shown) and find that the accessible area at the percolation threshold is an increasing function of N; i.e., the accessible area required for percolation increases with increasing N. This is because a bigger portion of the accessible area becomes nonpercolating as N is increased. As shown in Fig. 6, the nonpercolating accessible area fraction ϕ_{np} increases with increasing N. Therefore, even though ϕ_{acc} increases with N, ϕ_{np} also increases, which results in the nonmonotonic behavior in ϕ_c.

The simulations argue against the disklike model for chain conformations in two dimensions. If 2D polymers were disklike a longer chain would form a bigger disklike molecule. For a fixed value of ϕ_m, longer chains form a fewer number of disklike molecules but with a larger diameter thus providing monomers with a larger percolating accessible area as N increases. This is not observed, however, in the simulations. Figure 7 depicts the percolating accessible area fraction ϕ_p as a function of ϕ_m. From $N=1$ to 2, ϕ_p increases significantly. For $N \geq 4$, ϕ_p is insensitive to N for a given ϕ_m and, in fact, decreases as N goes from 8 to 256. This implies that polymers are not disklike in two dimensions, which is consistent with the previous observation in MC simulations [12].

In three dimensions ϕ_c does not show a nonmonotonic dependence on N. Figure 8 shows that ϕ_c increases with N but reaches a plateau at $\phi_c=0.29$ beyond $N=8$. When monomers are linked via chemical bonds to synthesize longer polymers, the excluded volume usually decreases [26], which is why ϕ_c increases with N for small values of N. But this effect becomes less important for longer chains where chain ends are fewer (for a given value of ϕ_m). The saturation of the effect for relatively short chains ($N=8$), however, is surprising.

The transition of the percolation behavior from two dimensions to three dimensions occurs for small values of $h \approx 2$. Figure 9 depicts the pseudopercolating area fraction, ϕ_A, defined as $\phi_A \equiv Nn\pi\sigma_M^2/4L^2$ at the percolation threshold, as a function of N for various values of h. As h (the finite thickness in three dimensions) is increased from 1 to 2, the nonmonotonic behavior of the percolation threshold concentration becomes less pronounced and ϕ_A shows behavior similar to that observed in three dimensions for $h=2$.

IV. SUMMARY AND CONCLUSIONS

We study the distribution and connectivity of accessible area (volume) in polymer solutions. The pore size distribution of polymers is qualitatively different from that of monomers or dimers, with no peak at finite values of pore sizes (in polymeric media). The polymer volume fraction at pore percolation threshold is a nonmonotonic function of N in two dimensions with a maximum at $N=8$. This is because the accessible area fraction required for percolation increases as the chain length is increased. For large N a large fraction of accessible area is inside the molecules and does not contribute to the accessible area percolation. The percolating area fraction decreases with increasing N and corroborates that the polymer chains in two dimensions are not disklike. We investigate the transition from 2D to 3D behavior by studying chains confined between surfaces. The 3D behavior is recovered when the separation between the surfaces is twice the monomer diameter.

The investigation of the structure of void space provides useful insight not available from pair correlation functions because they depend on three body and higher correlation functions. Voronoi tessellation has proved to be a useful tool to study nonspherical molecules or polydisperse materials [31,40], and this algorithm should help study pore structures of realistic polymer materials.

ACKNOWLEDGMENTS

This material is based on work supported by the National Science Foundation under Grant No. CHE-0717569 to A.Y. This work was supported by the Korea Research Foundation Grant funded by the Korean Government (MOEHRD) (Grant No. KRF-2008-331-C00141). This work was also supported by the Sogang University Research Grant No. 20071116.

[1] J.-M. Leväsalmi and T. J. McCarthy, Macromolecules **30**, 1752 (1997).
[2] B. D. Freeman, Macromolecules **32**, 375 (1999).
[3] T. C. Merkel, B. D. Freeman, R. J. Spontak, Z. He, I. Pinnau, P. Meakin, and A. J. Hill, Science **296**, 519 (2002).
[4] Q. Deng, F. Zandiehnadem, and Y. C. Jean, Macromolecules **25**, 1090 (1992).
[5] V. P. Shantarovich, I. B. Kevdina, Y. P. Yampolskii, and A. Y. Alentiev, Macromolecules **33**, 7453 (2000).
[6] C. Nagel, E. Schmidtke, K. Günther-Schade, D. Hofmann, D. Fritsch, T. Strunskus, and F. Faupel, Macromolecules **33**, 2242 (2000).
[7] D. Rigby and R. J. Roe, Macromolecules **23**, 5312 (1990).
[8] F. W. Starr, S. Sastry, J. F. Douglas, and S. C. Glotzer, Phys. Rev. Lett. **89**, 125501 (2002).
[9] K. Süvegh, M. Klapper, A. Domján, S. Mullins, W. Wunderlich, and A. Vértes, Macromolecules **32**, 1147 (1999).
[10] M. Sega, P. Jedlovszky, and N. N. Medvedev, J. Chem. Phys. **121**, 2422 (2004).
[11] P. G. De Gennes, *Scaling Concepts in Polymer Physics* (Cornell University Press, Ithaca, NY, 1979).
[12] A. Yethiraj, Macromolecules **36**, 5854 (2003).
[13] P. Eggl, D. Pink, B. Quinn, H. Ringsdorf, and E. Sackmann, Macromolecules **23**, 3472 (1990).
[14] T. D. Sells and D. F. O'Brien, Macromolecules **27**, 226 (1994).
[15] S. I. Stupp, H. C. Son, and L. S. L. Lin, Science **259**, 59 (1993).
[16] T. M. Sisson, H. G. Lamparski, S. Kölchens, A. Elayadi, and D. F. O'Brien, Macromolecules **29**, 8321 (1996).
[17] S. Kölchens, H. Lamparski, and D. F. O'Brien, Macromolecules **26**, 398 (1993).
[18] A. R. Kerstein, J. Phys. A **16**, 3071 (1983).
[19] S. Torquato and S. B. Lee, Physica A **167**, 361 (1990).
[20] S. S. Rane and P. D. Gujrati, J. Chem. Phys. **116**, 3947 (2002).
[21] X. Wang, K. M. Lee, Y. Lu, M. T. Stone, I. C. Sanchez, and B. D. Freeman, Polymer **45**, 3907 (2004).
[22] P. in 't Veld, M. T. Stone, T. M. Truskett, and I. C. Sanchez, J. Phys. Chem. B **104**, 12028 (2000).
[23] H. Wittmann, K. Kremer, and K. Binder, J. Chem. Phys. **96**, 6291 (1992).
[24] A. Okabe, B. Boots, K. Sugihara, and S. N. Chiu, *Spatial Tessellations* (Wiley, New York, 2000).
[25] S. Arizzi, P. H. Mott, and U. W. Suter, J. Polym. Sci., Part B: Polym. Phys. **30**, 415 (1992).
[26] M. L. Greenfield and D. N. Theodorou, Macromolecules **26**, 5461 (1993).
[27] L. Xu, T. T. Tsotsis, and M. Sahimi, J. Chem. Phys. **114**, 7196 (2001).
[28] L. Xu, M. Sahimi, and T. T. Tsotsis, Phys. Rev. E **62**, 6942 (2000).
[29] S. L. Bryant, P. R. King, and D. W. Mellor, Transp. Porous Media **11**, 53 (1993).
[30] S. Putta and S. Nemat-Nasser, Mater. Sci. Eng., A **317**, 70 (2001).
[31] V. A. Luchnikov, N. N. Medvedev, L. Oger, and J. P. Troadec, Phys. Rev. E **59**, 7205 (1999).
[32] A. V. Anikeenko, M. G. Alinchenko, V. P. Voloshin, N. N. Medvedev, M. L. Gavrilova, and P. Jedlovszky, Lect. Notes Comput. Sci. **3045**, 217 (2004).
[33] N. Tokita, M. Hirabayashi, C. Azuma, and T. Dotera, J. Chem. Phys. **120**, 496 (2004).
[34] B. J. Sung and A. Yethiraj, Phys. Rev. Lett. **96**, 228103 (2006).
[35] B. J. Sung and A. Yethiraj, J. Phys. Chem. B **112**, 143 (2008).
[36] B. J. Sung and A. Yethiraj, J. Chem. Phys. **128**, 054702 (2008).
[37] A. Yethiraj and C. K. Hall, Macromolecules **23**, 1865 (1990).
[38] F. T. Wall and F. Mandel, J. Chem. Phys. **63**, 4592 (1975).
[39] J. J. De Pablo, M. Laso, and U. W. J. Suter, J. Chem. Phys. **96**, 2395 (1992).
[40] M. G. Alinchenko, A. V. Anikeenko, N. N. Medvedev, V. P. Voloshin, M. Mezei, and P. Jedlovszky, J. Phys. Chem. B **108**, 19056 (2004).